BUTTERWORTH HEINEMANN

Polymer Vol. 36 No. 13, pp. 2541–2552, 1995

0032-3861/95/$10.00 + 0.00

Fracture toughness of a polycarbonate/acrylonitrile–butadiene–styrene blend by the ASTM E813 and hysteresis energy *J* integral methods: effect of specimen thickness and side groove

Ming-Luen Lu and Feng-Chih Chang*
Institute of Applied Chemistry, National Chiao Tung University, Hsinchu 30050, Taiwan, Republic of China
(Received 11 May 1994; revised 19 August 1994)

A previously developed non-conventional *J* integral based on hysteresis energy and the ASTM E813 methods have been employed to test the fracture toughness of a polycarbonate (PC)/acrylonitrile–butadiene–styrene (ABS) blend. A systematic study of the effect of the specimen thickness (from $B=4$ to 15 mm) and the presence of a V-shaped side groove on the resultant J_{1c} has been carried out. The results show that the J_{1c} values obtained from the hysteresis energy method and the E813-81 method are comparable, but are ~60–90% lower than those obtained from the E813-87 method. When the specimen thickness is relatively thin, the J_{1c} values obtained from the V-shaped-side-grooved specimens are slightly higher than those from samples without the side groove, but this difference gradually decreases with an increase in the specimen thickness. The J_{1c} values obtained from the ungrooved specimens are almost independent of the specimen thickness (from $B=4$ to 15 mm) for all of these methods. The critical initiation displacements in terms of the onset of crack initiation, determined from the plots of hysteresis energy *versus* displacement, hysteresis ratio *versus* displacement, and crack growth length *versus* displacement, are fairly close in value. This means that the critical crack initiation and the corresponding J_{1c} obtained from this hysteresis energy method indeed represent the actual physical event of the onset of crack initiation.

(Keywords: fracture toughness; *J* integral method; PC/ABS blend)

INTRODUCTION

Linear elastic fracture mechanics (LEFM) is now widely used to characterize the fracture behaviour of many polymer materials. The size- and geometry-independent parameters, K_{1c} and G_{1c}, have been shown to present the true material constants of most brittle polymers[1], provided that certain restrictive size criteria of the testing specimen have been satisfied in order to meet the requirements of the plane-strain fracture. In these cases, the energy dissipation is only limited locally to the crack tip region so that the behaviour of the bulk material is still elastic and the fracture behaviour can be derived from the energy change in an elastic analysis. However, when the extent of the plastic deformation increases for those more ductile materials, these LEFM parameters, K_{1c} and G_{1c}, are eventually inapplicable. During the last two decades, a considerable effort has been dedicated to characterizing the fracture behaviour of more ductile materials or structural materials employed at temperatures where they exhibit an elastic–plastic behaviour. This effort has focused on the *J* integral method, which was originally proposed by Rice[2] as a means of characterizing the stress–strain singularity at a crack tip in an elastic or elastic–plastic material. Begley and Landes[3,4] applied the *J* integral concept and developed a measurement of the fracture toughness, J_{1c}, which represents the energy required to initiate the crack growth. During the last decade, *J* integral methods have been applied successfully to numerous ductile polymeric materials[5–18] using the multiple-specimen method developed by Begley and Landes[3] or the single-specimen method developed by Rice *et al.*[19]. The crack growth in the single-specimen method is measured by using an elastic unloading compliance technique[19]. However, the crack growth measured from the side-view may not be accurate because the crack front may vary from the central region to the side sections. Therefore, the *J* values evaluated by using this single-specimen method do not always agree with the values obtained from the standard multiple-specimen method. Westerlind *et al.*[20] reported that the critical *J* values obtained by using this single-specimen method were greater than those obtained from the standard multiple-specimen technique. A critical value of the *J* integral, J_{1c}, has been commonly used to characterize ductile fracture in materials exhibiting large-scale yielding[21,22]. Two key ASTM Standards, namely E813-81 and E813-87, were established for *J*-testing procedures, mainly for metallic materials[23,24] and these have also been extended to

* To whom correspondence should be addressed

characterize various toughened polymers and blends during the last decade[5–18]. However, the optimum procedures of the test have not yet been conclusively defined and standardized. Subsequently, several different approaches for J integral testing have been developed. Seidler and Grellmann[25] studied the fracture behaviour and morphologies of polycarbonate (PC)/acrylonitrile–butadiene–styrene (ABS) blends using a special technique, i.e. a stop-block method. Mai and coworkers[26–28] used the essential work method to characterize the fracture toughness of many tough polymers. Zhou *et al.*[29] used the single-specimen normalization method to develop J–R curves and to characterize the toughness of polymeric materials for which the direct measurement of the crack growth length is not required. This normalization method uses the plastic deformation character of the material to determine indirectly the crack extension. Chung and Williams[30] used the elastic compliance method to calculate the crack growth in three-point bending experiments on single specimens of poly(vinylidine difluoride). A series of hysteresis loops have been observed during the load–unloading cycles, which indicates the viscoelastic and/or inelastic nature of the polymer. The accurate measurement of the crack extension by this elastic compliance method is difficult to achieve, and therefore it is rather questionable that this method is a reliable technique for constructing the J–R curve in the single-specimen method. In fact, when a precracked specimen of a toughened polymer is under load, various viscoelastic and inelastic micromechanisms such as crazing, cavitation, debonding and shear yielding may significantly occur around the crack tip region. A significant fraction of the energy embodied in J is dissipated viscoelastically or inelastically before crack extension occurs. Therefore, it would be desirable to develope a non-conventional hysteresis energy method to characterize the fracture toughness of ductile polymeric materials. In our recent studies on the fracture toughness of elastomer-toughened polycarbonate, acrylonitrile–butadiene–styrene (ABS), and high impact polystyrene (HIPS), an unconventional approach to the J integral, based on the above mentioned hysteresis properties, was employed[31–35]. This newly developed hysteresis energy method does not have any of the drawbacks of the single-specimen method and is complementary with the existing ASTM standard methods. In this present paper, the hysteresis energy method and the ASTM standards E813-81 and E813-87 are used to characterize the fracture toughness of a PC/ABS blend.

CHARACTERIZING PARAMETERS OF FRACTURE MECHANICS

The J integral

Rice[2] developed the path-independent energy line integral, the J integral, which is an energy-based parameter, to characterize the stress–strain field near a crack tip surrounded by small-scale yielding. The J integral is defined by the following equation:

$$J=\int_{\Gamma}\left(\bar{W}\mathrm{d}y-\bar{T}\frac{\partial\bar{U}}{\partial x}\mathrm{d}S\right) \tag{1}$$

where Γ is any path around the crack tip of the specimen, $\bar{T}$ is the surface traction, $\bar{W}$ is the strain energy density,

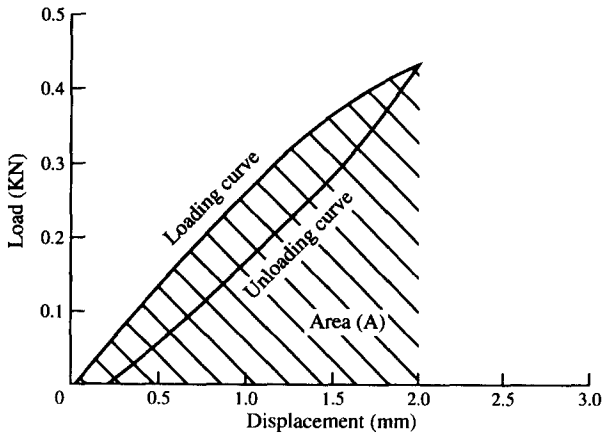

Figure 1 ASTM SENB loading–unloading curve; the hatched area, A, is used to approximate the J integral, i.e. $J=2A/(Bb)$

$\bar{U}$ is the displacement vector, and x and y are the axis coordinates. Rice[2] and Begley and Landes[3,4] showed that the J integral can be interpreted as the potential energy change with crack growth, which can be expressed by the following equation:

$$J=-\frac{\mathrm{d}U}{B\mathrm{d}a} \tag{2}$$

where B is the thickness of the loaded body and a is the crack length; U is the total potential energy, which can be obtained by measuring the area under the load–displacement curve (*Figure 1*). However, for large-scale yielding, the potential energy U does not represent the energy available for crack growth, but rather the work done in deforming the specimen.

ASTM Standard methods

The multiple-specimen method is based directly on the interpretation of the J integral as expressed by equation (2). Sumpter and Turner[36] later expanded this equation and rewrote it in the following form:

$$J=J_{\mathrm{e}}+J_{\mathrm{p}} \tag{3}$$

J_{e} and J_{p} are the elastic and plastic components, respectively, of the total J value, and can be expressed by the following equations:

$$J_{\mathrm{e}}=\frac{\eta_{\mathrm{e}}U_{\mathrm{e}}}{B(W-a)} \tag{4}$$

$$J_{\mathrm{p}}=\frac{\eta_{\mathrm{p}}U_{\mathrm{p}}}{B(W-a)} \tag{5}$$

where U_{e} and U_{p} are the elastic and plastic components, respectively, of the total energy, η_{e} and η_{p} are their corresponding elastic and plastic work factors, $(W-a)$ is the ligament length and W is the specimen width. For a three-point bend, single-edge notched specimen with $a/W>0.15$, η_{p} is equal to 2. When the specimen has a span of $4W$ ($S=4W$) and $0.4<a/W<0.6$, η_{e} is also equal to 2. Therefore equation (3) can be reduced to the following:

$$J=\frac{2U}{B(W-a)} \tag{6}$$

where b is the ligament length. The crack growth

resistance (R-curve) is obtained by plotting the J values against the corresponding Δa values.

In the ASTM E813-81 Standard, the critical J value for crack initiation, J_{1c}, is determined by intersecting the linear regression R-curve and the crack blunting line. The blunting line can be expressed by the following equation:

$$J = 2m\sigma_y \Delta a \tag{7}$$

where Δa is the crack growth length, σ_y is the yield strength, and m is a constraint factor ($m=1$ for plane stress and $m=2$ for plane strain). Two lines parallel to the crack blunting line at an offset of $0.006b$ and $0.06b$ (mm) are drawn respectively as the minimum and maximum crack extension lines[23].

In the ASTM E813-87 Standard, instead of a bilinear fitted line, the J–Δa curve is fitted by using a power law, according to the following equation[24]:

$$J = C_1 \Delta a^{C_2} \tag{8}$$

The critical J value, J_{1c}, is now located at the intersection of the power-law-fitted line and the 0.2-mm-blunting-offset line represented by the following equation:

$$J = 2\sigma_y \Delta a - 0.4\sigma_y \tag{9}$$

The J_{1c} validity requirements

For the fracture to be characterized as J_{1c}, a specimen must meet certain size requirements in order to achieve a plane strain–stress stage along the crack front. To achieve this stress state, all specimen dimensions must exceed some multiple of J_{1c}/σ_y. According to ASTM E813[23,24], a valid J_{1c} value may be obtained, whenever the following is achieved:

$$B,\ (W-a),\ W > 25\left(\frac{J_{1c}}{\sigma_y}\right) \tag{10}$$

Paris *et al.*[37] developed the tearing modulus concept to describe the stability of a ductile crack in terms of elastic–plastic fracture mechanics. This fracture instability occurs if the elastic shortening of the system exceeds the corresponding plastic lengthening for crack extension. A non-dimensional parameter, the tearing modulus (T_m), has been defined by the following equation[37]:

$$T_m = \left(\frac{dJ}{da}\right)\left(\frac{E}{\sigma_y^2}\right) \tag{11}$$

Furthermore, for the J–Δa data to be regarded as a material property which is independent of specimen size, the criterion $\omega > 10$ must be met, where ω is defined as follows:

$$\omega = \frac{(W-a)}{J_{1c}} \cdot \left(\frac{dJ}{da}\right) \tag{12}$$

J integral according to the hysteresis energy method

There are many practical cases in laboratory tests where it is necessary to evaluate a grossly non-linear dissipative system. Such situations have been treated by Andrews and coworkers[38,39] using a generalized theory. However, this approach requires complicated and time-consuming experiments and involves some assumptions concerning the nature of the hysteresis behaviour. According to Andrew's generalized fracture mechanics theory[38,39], the fracture energy of a solid is given by the following:

$$\mathcal{J} = \mathcal{J}_0 \Phi(\varepsilon_0, \dot{a}, T) \tag{13}$$

where $\mathcal{J}$ is the total fracture energy of the system needed to cause a unit area of crack growth; $\mathcal{J}_0$ is the intrinsic fracture energy (or surface energy) to rupture a unit area of interatomic bonds across the fracture plane, and Φ is a loss function depending on the crack velocity $\dot{a}$, the temperature T, and the applied strain ε_0. The loss function is derived as follows:

$$\Phi = \frac{K_1(\varepsilon_0)}{\left[K_1(\varepsilon_0) - \frac{1}{2}\sum_{PU} \beta(xy) g \delta_x \delta_y\right]} \tag{14}$$

where K_1 is a function of strain, x and y are the reduced cartesian coordinates of the point P, $\beta(x, y)$ is the hysteresis ratio at the point P, and the symbol PU denotes summation over points which unload as the crack propagates. The evaluation of the term $\sum_{PU} \beta(x, y) g \delta_x \delta_y$ of equation (14) requires an additional knowledge of the hysteresis ratio β from point to point in the stress field, and β will in general be a function of the local strain, strain rate, and temperature. We have assumed that β is a unique function of input energy density at a given strain rate.

The hysteresis defined in this hysteresis energy method is not exactly the same as that in the above definition; it is the energy difference between the input and the recovery in the cyclic loading and unloading steps, which may include crack blunting and crack extension stages (as shown in *Figure 1*). The energy density change during crack growth can be presented as the following equation:

$$\frac{dU}{dA} = aW_0\left[\left(\sum_{PL} g(xy)\delta_x\delta_y\right) - \left(\sum_{PU} G(xy\sigma_y)\right)\delta_x\delta_y\right] \tag{15}$$

where PL and PU indicate loading and unloading, respectively; W_0 is the input energy density, a is the precrack length, and g and G are functions of x, y, and σ_y. The quantity of the first term in the right-hand side of equation (15) includes the energy available for forming a crack surface and the energy consumed in a plastic deformation of the cracked specimen. The input energy density W_0 can be given by the area (A_0) under the loading curve up to a particular strain ε, and the recoverable energy density W_r is the area under the unloading range covered (A_r). The hysteresis ratio (HR) is then defined by the following equation:

$$HR = \frac{A_0 - A_r}{A_0} \tag{16}$$

and the hysteresis energy (HE) is given as follows:

$$HE = HRU \tag{17}$$

where U is the input energy at different displacements.

For a cracked specimen under loading, the material surrounding the crack tip can be divided into three regions, as shown in *Figure 2a*: ⟨1⟩ the primary plastic zone, ⟨2⟩ the secondary plastic zone, and ⟨3⟩ the fracture surface. The specific energy balance equation for a

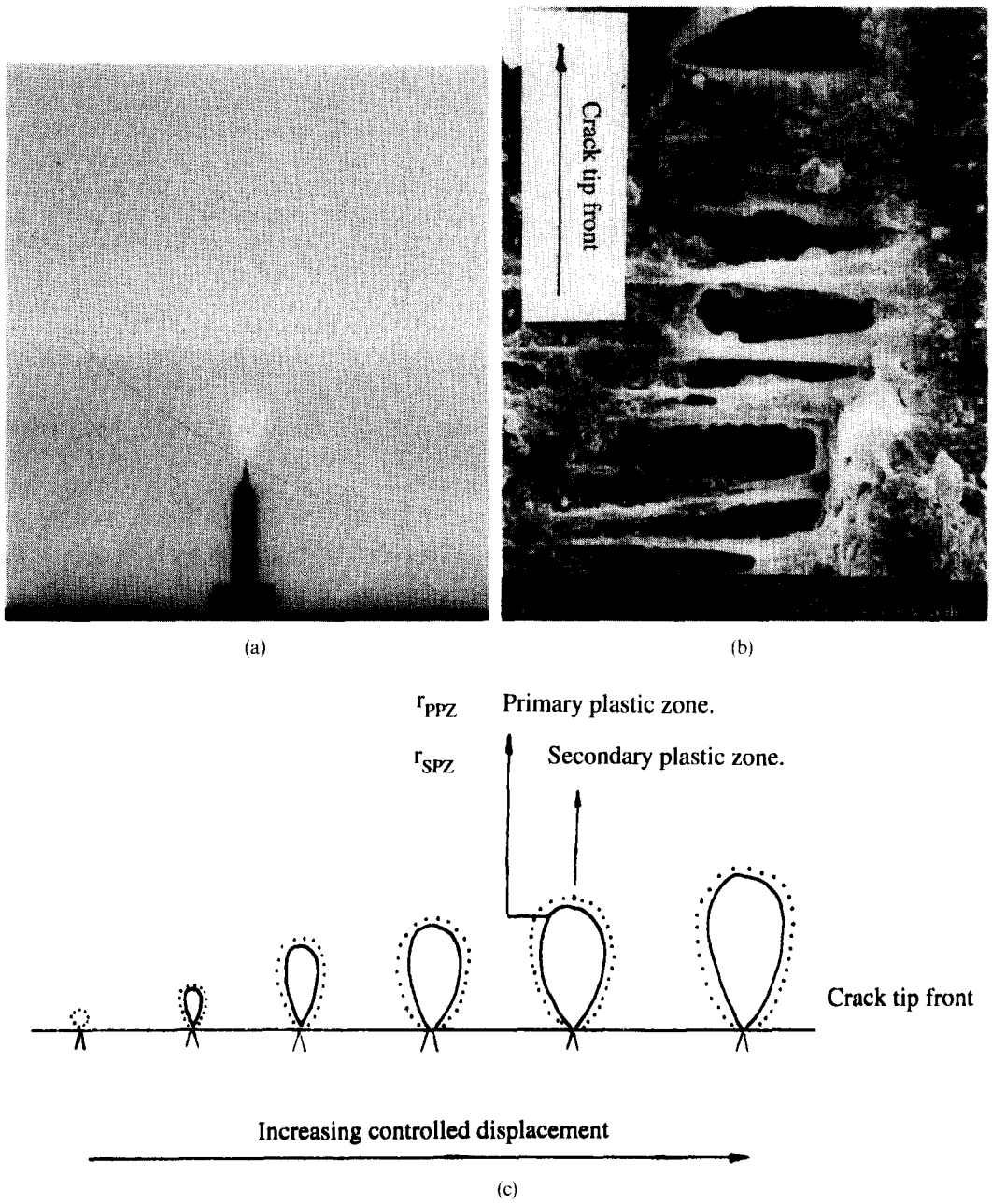

Figure 2 (a) Side-view optical photograph of the central region of a PC/ABS specimen (with $B = 8$ mm). (b) Scanning electron micrograph of the crack tip region of the same sample. (c) Schematic representation of the growth of the plastic zones (see text for details)

cracked specimen can be expressed by the following:

$$\frac{1}{B}\left(\frac{dU}{da}-\frac{dU_e}{da}-\frac{dU_k}{da}\right)=\frac{1}{B}\left(\frac{dU_P^{PPZ}}{da}+\frac{dU_P^{SPZ}}{da}\right)+2\gamma_s \tag{18}$$

and the energy dissipated for a unit crack growth area of the system is given as follows:

$$\frac{dHE}{dA}=\frac{1}{B}\left(\frac{dU_P^{PPZ}}{da}+\frac{dU_P^{SPZ}}{da}\right)+2\gamma_s \tag{19}$$

where U_k is the kinetic energy, U_e is the elastic energy, U_p^{PPZ} is the plastic energy for the primary plastic zone, U_P^{SPZ} is the plastic energy for the secondary plastic zone, and γ_S is the fracture surface energy. The close relationship between the precrack hysteresis and the corresponding ductile–brittle transition behaviour of polycarbonate and polyacetal has been reported[40–43]. When a precrack specimen is under loading before the onset of crack extension (during blunting), a significant portion of the input energy is consumed and converted into a relatively larger crack tip plastic zone (for toughened polymers). These viscoelastic and inelastic energies may include the effects of many possible energy dissipation micromechanisms, such as crazing, cavitation, debonding, and shear yielding, which can be related to the measured hysteresis energy. The hysteresis energy will increase gradually with an increase of load or displacement as can be seen from the load *versus* displacement curve. After crack extension, the strain energy release due to crack growth will be added to the observed total hysteresis energy. The rate of hysteresis energy increase due to this strain energy release is significantly higher than those resulting from the above

mentioned precrack micromechanisms. Therefore, in a plot of hysteresis energy *versus* deformation displacement of a notched specimen, a clear transition from a crack blunting to crack extension can be identified. Such a phenomenon, namely a faster rate of the hysteresis energy increase immediately after the onset of the crack extension, can be used to determine the critical fracture toughness (J_{1c}) at the onset of crack extension. The data observed which support this viewpoint have been presented in our previous papers[31–35].

EXPERIMENTAL

The PC/ABS blend (Shinblend A783) was obtained from Shing-Kong Synthetic Fiberic Corporation of Taiwan. Two groups of test specimens of the three-point bending bars, with and without the V-shaped side groove, were employed. The specimens used had a width (w) of 20 mm, and a length (l) of 90 mm, while the thickness (B) varied from 4 to 15 mm. The first group of ungrooved specimens, with a single-edge notch of an initial crack length a of 10 mm ($a/W=0.5$) were prepared by injection moulding, using an Arburg injection moulding machine (*Figure 3*). The second group of grooved specimens were prepared from the ungrooved samples by cutting out V-shaped side grooves by using a flying cutter (*Figure 3*). The initial precrack was then followed by sharpening with a fresh razor blade. All of the notched specimens were annealed at 80°C for 2–3 h in order to release any possible residual stress, prior to the standard bending tests. The J method was carried out according to the ASTM E813 Standard at a crosshead speed of 2.0 mm min^{-1} by using a universal tensile testing machine (Instron Model 4201). The specimens were loaded to various displacements corresponding to different crack growth lengths and then unloaded at the same test rate. After fully unloading, the specimens were frozen in liquid nitrogen and broken open by a TMI impacter. The crack growth length of the broken specimen, Δa, was measured by using a travelling optical microscope. The input and hysteresis energies of each test specimen were obtained by measuring the areas under the load–displacement curves and the energy loss from the loading–unloading loop, respectively.

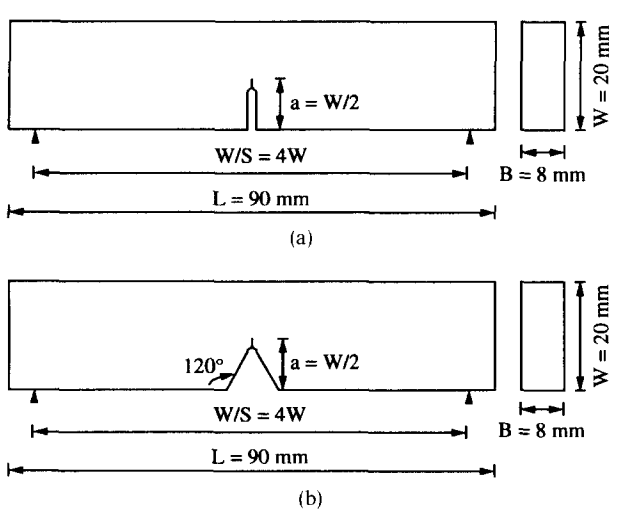

Figure 3 Geometry of injection moulded specimens: (a) without side groove; (b) with V-shaped side groove

RESULTS AND DISCUSSION

Photographic studies

Figure 2a shows the side-view optical photograph of the central section of a specimen ($B=8$ mm) which had been carefully polished to approximately half of its original thickness and then viewed by optical microscopy. The scanning electron micrograph (*Figure 2b*) of the crack tip front region shows the craze-like failure. Two plastic zones can be identified around the crack (in terms of the degree of stress whitening): the interior one is the primary plastic zone (indicated in *Figure 2c*) while the outer one is the secondary plastic zone (see *Figure 2c*). The secondary plastic zone is a diffuse zone surrounding the primary plastic zone. Both plastic zones have an elliptical shape which surrounds and extends from the crack tip. *Figure 2c* shows a schematic plot of the gradual growth of these plastic zones for a PC/ABS blend with an 8 mm thickness. The secondary zone represents the material being partially damaged under triaxial tensional stress prior to reaching the fully developed plastic deformation stage. This secondary zone always travels in front of the primary plastic zone, and, in fact, it appears first at the early stage of loading, before the appearance of the primary plastic zone. This partially damaged secondary zone may involve rubber cavitations, crazing, and rubber-induced localized shear yielding but the majority of the material is just close to, but not quite at the yield point. The fracture surface is schematically illustrated in *Figure 4a*, where the crack growth length (between lines A and B) is fairly consistent from the centre to the skin of the specimen. The crack tip stress whitening zone (between lines B and C) is considered as the primary plastic zone. The boundaries between the primary plastic/secondary plastic/undamaged zones cannot be clearly distinguished from the fracture surface. *Figures 4b–d* show, respectively, the detailed scanning electron micrograph features of the crack growth, the primary plastic zone, and the undamaged zone (or possibly the diffused secondary plastic zone) of the cryogenically fractured surface. The crack growth zone (*Figure 4b*) shows characteristics of surface tearing along the crack growth direction with extensively localized shear yielding. The primary plastic zone (*Figure 4c*) shows more of the rough fracture surface than the undamaged zone (or diffused secondary plastic zone) (*Figure 4d*). The latter shows a typical brittle fracture surface as a result of the specimen being frozen in liquid nitrogen prior to fracture.

J_{1c} determination by ASTM Standards and their modified versions

The complete fracture load–displacement curves of the notched specimens (without the side groove) with various thicknesses are shown in *Figure 5*. The specimen with the highest thickness has a considerably higher maximum load than the thinner specimens. The multiple-specimen technique is employed by loading the specimen to a controlled displacement on the curve and then unloading according to the ASTM method. The J value for each specimen at each controlled displacement is calculated by using equation (6) and the corresponding crack growth (Δa) is measured from the surface of the broken specimen. Detailed data for the specimens with $B=8$ mm (without the side groove) are summarized in *Table 1*. *Figure 6*

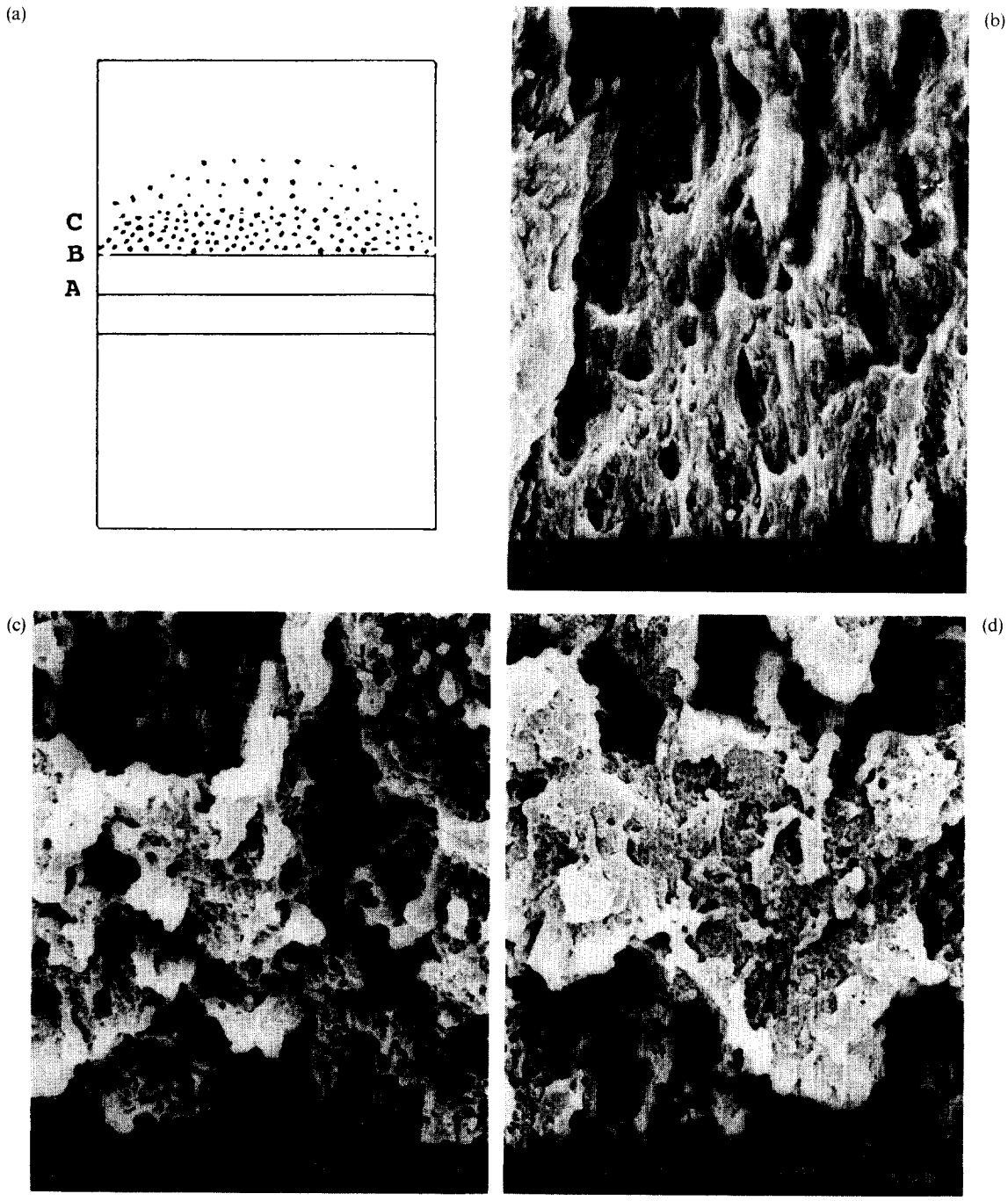

Figure 4 Fracture surfaces of a PC/ABS blend with $B = 8$ mm: (a) schematic representation of the fracture surface showing the various zones; (b) scanning electron micrograph of the crack growth zone (between lines A and B); (c) scanning electron micrograph of the stress whitening zone (between lines B and C); (d) scanning electron micrograph of the undamaged zone (or secondary plastic zone) (above line C)

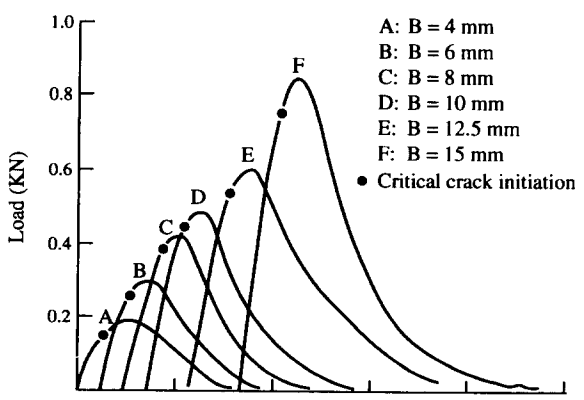

Figure 5 Load–displacement curves obtained for PC/ABS samples of different thicknesses

shows plots of the acceptable J *versus* Δa, using results obtained from the linear regression R-curves according to the ASTM E813-81 method, for PC/ABS specimens ($B = 8$ mm) with and without the V-shaped side groove. The linear regression R-curves intercept with the blunting line (equation (7)) to locate the J_{1c} values. Another critical J value (J_0) can be determined from the interception of the linear regression resistance curve with the y-axis, as suggested by Narisawa and Takemori[16]; this give values which are slightly lower than those obtained from the E813-81 method, as would be expected. However, the resistance curve (and its slope) obtained for the V-shaped side-grooved specimens is slightly higher than for those without the side groove. This observed

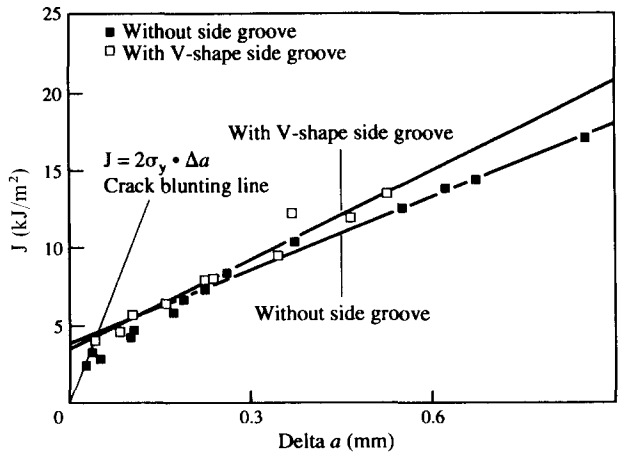

Figure 6 J integral curves obtained by the ASTM E813-81 method for PC/ABS specimens with and without the V-shaped side grooves

Table 1 J data obtained for a typical PC/ABS blend with $B = 8$ mm

D^a (mm)	Input energy (J)	J^b (kJ m^{-2})	Hysteresis ratio (%)	Hysteresis energy (J)	Δa^c (mm)
0.8	0.051	1.275	2.91	0.0016	-
1.0	0.096	2.400	3.75	0.0036	0.026
1.2	0.118	2.950	4.77	0.0056	0.047
1.3	0.128	3.200	5.21	0.0066	0.037
1.4	0.173	4.325	7.22	0.0125	0.107
1.5	0.189	4.725	8.83	0.0167	0.106
1.6	0.233	5.825	12.57	0.0293	0.170
1.7	0.262	6.550	11.78	0.0309	0.186
1.8	0.297	7.425	14.66	0.0435	0.223
1.9	0.336	8.400	18.14	0.0610	0.260
2.1	0.415	10.375	25.27	0.1049	0.371
2.3	0.507	12.675	29.80	0.1511	0.550
2.4	0.577	14.625	32.34	0.1866	0.670
2.5	0.552	13.800	35.41	0.1955	0.625
2.7	0.683	17.075	41.95	0.2865	0.852
2.8	0.739	18.475	43.25	0.3196	0.877
2.9	0.765	19.125	47.89	0.3664	0.912
3.0	0.859	21.475	50.33	0.4323	1.141

[a] Deformation displacement
[b] $J = 2U/(Bb)$
[c] Measured crack growth length

Table 2 Critical J values obtained from ASTM E813-81 methods for specimens with and without the V-shaped side grooves

Without side groove						
Thickness B (mm)	4	6	8	10	12.5	15
J_{1c} (kJ m^{-2})[a]	3.81	4.31	4.28	4.38	3.87	3.55
J_o (kJ m^{-2})[b]	3.26	3.72	3.62	3.36	3.12	3.00
With V-shaped side groove						
Thickness B (mm)	4	6	8	10	12.5	15
J_{1c} (kJ m^{-2})[a]	6.56	5.42	4.26	4.57	3.64	3.45
J_o (kJ m^{-2})[b]	5.53	4.52	3.47	3.83	2.99	2.89

[a] J_{1c} obtained by standard ASTM E813-81 method
[b] J_o obtained by a modified version of the ASTM E813-81 method by intercepting the blunting line with the y-axis

difference can be attributed to the expected constraint of the V-shaped side-grooved specimens relative to the ungrooved samples. All these data, obtained from ASTM E813-81 and the modified methods by varying the specimen thickness, are summarized in *Table 2*. *Figure 7* shows plots of the J_{1c} values *versus* specimen thickness, for samples with and without the V-shaped side groove. The values obtained from the specimens with side grooves are higher than those without for specimen thicknesses less than 8 mm. However, the J_{1c} values obtained are roughly equal, and independent of specimen thickness, for values of B from 8 to 15 mm, for both sample geometries. In the ASTM E813-87 method, the values of C_1 and C_2 of the power-law regression line, $J = C_1 \Delta a^{C_2}$, are obtained from the plot of ln J *versus* ln Δa within the exclusion lines between $\Delta a = 0.15$–1.5 mm, as shown in *Figure 8*. J_{1c} is then located at the intercept between the power-law fitted line and the 0.2 mm offset line (equation (9)), as shown in *Figure 9* for $B = 8$ mm. The J_{1c} values for different specimen thicknesses, ranging from $B = 4$ to 15 mm for both sample geometries, are summarized in *Table 3*. *Figure 10* shows the plots of the critical fracture toughness (J_{1c}) *versus* specimen thickness using results obtained from the ASTM E813-87 method for both V-shaped grooved and ungrooved specimens. Again, the J_{1c} values obtained for the grooved specimens are higher than those of the ungrooved samples. The presence of the side groove decreases the crack tip constraint in the specimen. The J_{1c} values obtained from the E813-87 method are about 80–100% higher than those obtained from the corresponding E813-81 produce (see *Table 2*). The significantly higher J_{1c} values obtained from ASTM E813-87 when compared to the J_{1c} values

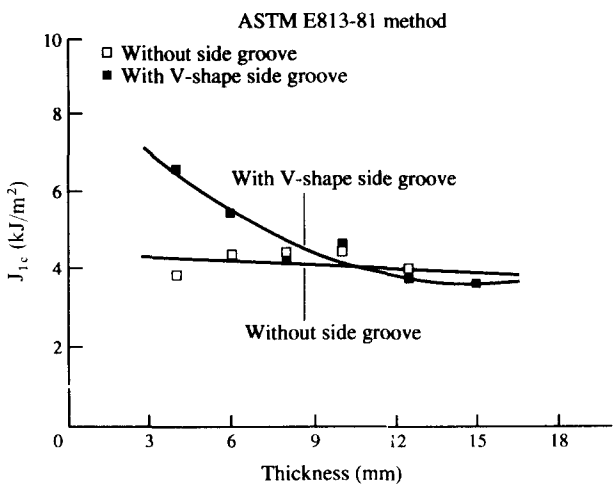

Figure 7 Plots of critical fracture toughness J_{1c} *versus* thickness obtained from the ASTM E813-81 method for PC/ABS samples with and without the V-shaped side grooves

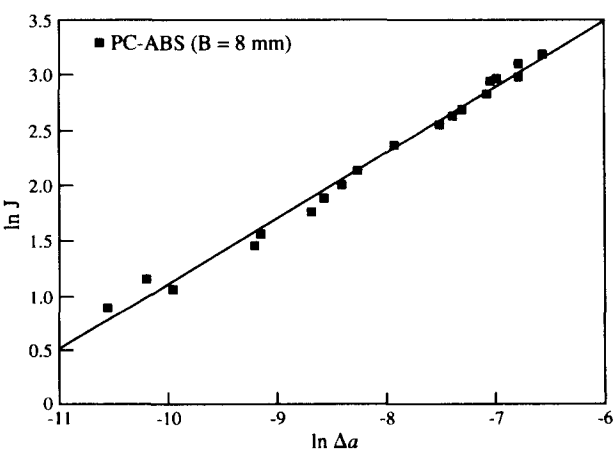

Figure 8 Plot of ln J *versus* ln Δa for a PC/ABS sample with $B = 8$ mm

Table 3 Critical J values obtained from the ASTM E813-87 method for specimens with and without the V-shaped side grooves

Without side groove						
Thickness B (mm)	4	6	8	10	12.5	15
C_1	1246	650	1102	1573	2323	1622
C_2	0.627	0.545	0.591	0.645	0.690	0.651
J_{1c} (kJ m^{-2})[a]	7.82	7.56	8.17	8.14	8.00	7.85
J_0 (kJ m^{-2})[b]	5.01	5.56	6.51	5.56	5.27	5.28
With V-shaped side groove						
Thickness B (mm)	4	6	8	10	12.5	15
C_1	2546	541	331	404	514	622
C_2	0.681	0.496	0.443	0.464	0.497	0.535
J_{1c} (kJ m^{-2})[a]	10.0	9.86	9.79	9.41	9.36	8.56
J_0 (kJ m^{-2})[b]	7.52	7.54	7.51	7.35	6.72	6.00

[a] J_{1c} obtained by standard ASTM E813-87 method
[b] J_0 obtained by a modified version of the ASTM E813-87 method by using a 0.1 mm offset line

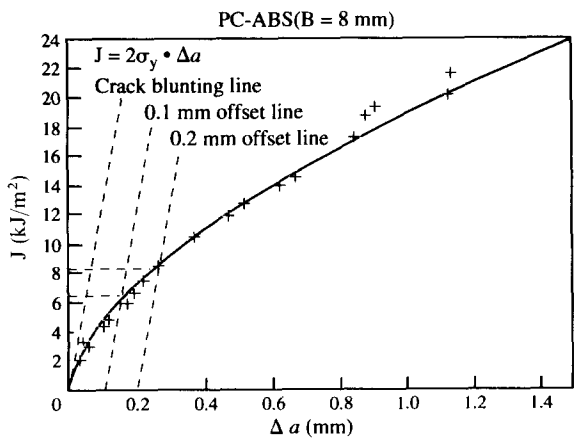

Figure 9 J integral plot obtained by the ASTM E813-87 method for a PC/ABS sample with $B=8$ mm

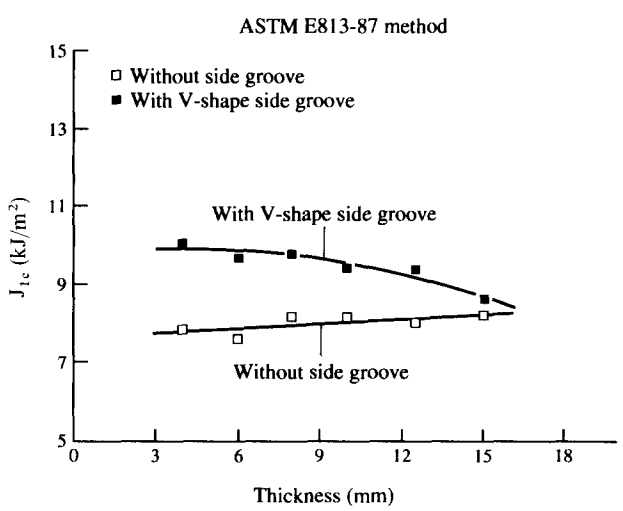

Figure 10 Plots of critical fracture toughness J_{1c} *versus* thickness for PC/ABS samples with and without V-shaped side grooves, obtained by the ASTM E813-87 method

obtained from E813-81 are a consequence of the J_{1c} values obtained from the former method not being evaluated from the real onset of crack growth (as defined by the blunting line), but from a finite amount of stable crack growth, i.e. $\Delta a=0.2$ mm. The critical J_{1c} definition has been a confusing and controversial issue, namely

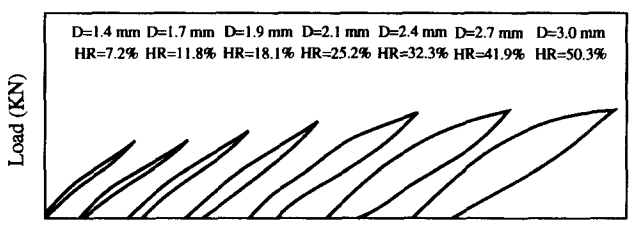

Figure 11 Plots of hysteresis loops at different controlled displacements for PC/ABS samples with $B=8$ mm

whether it is more appropriate for it to be treated as a crack initiation (E813-81) or simply as an engineering definition for design purposes (E813-87). However, if the 0.2 mm offset line, specified in E813-87, is now reset at 0.1 mm and the remaining procedures remain unchanged, then the critical J_0 values obtained from the E813-87 modified method are only slightly higher than those obtained from the E813-81 method (see *Table 2*). Similar results were also obtained from elastomer-modified polycarbonate[31], high impact polystyrene[33], and acrylonitrile–butadiene–styrene[35]. The 0.2 mm offset line suggested in the ASTM E813-87 standard is, after all, only an arbitrarily selected value which is used to define the critical fracture toughness (J_{1c}).

J_{1c} *determination from the hysteresis energy method*

Figure 11 illustrates the hysteresis loops and their corresponding hysteresis ratios at various stages of displacement for PC/ABS samples with $B=8$ mm. The hysteresis ratio and energy of each specimen at different displacements are calculated by equations (16) and (17), respectively. The results obtained for the hysteresis ratio and energy at different displacements are summarized in *Table 1*. The experimentally measured hysteresis energy is believed to be higher than the true hysteresis energy at the starting point of unloading because of the time-dependent viscoelastic nature of polymeric materials. It is impossible to obtain the true hysteresis energy experimentally at the end point of loading. However, with the crosshead speed used in this study, the difference between the true and the experimentally obtained hysteresis energies is considered to be negligible. We have assumed that the hysteresis ratio is a unique function of the input energy density at a given deformation. *Figure 12* shows plots of the hysteresis

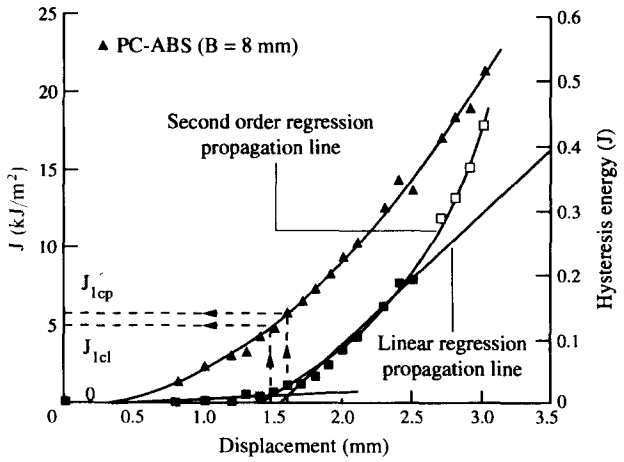

Figure 12 J integral curves obtained by the hysteresis energy method for PC/ABS samples with $B = 8$ mm

Table 4 Critical displacement[a] and corresponding J values obtained from the hysteresis energy method for a PC/ABS specimen with and without V-shaped side grooves

Without side groove						
Thickness B (mm)	4	6	8	10	12.5	15
D_{cl} (mm)	1.50	1.53	1.56	1.49	1.52	1.51
J_{1cl} (kJ m^{-2})	5.59	6.07	5.78	5.75	6.06	5.82
D_{cp} (mm)	1.40	1.38	1.41	1.28	1.25	1.36
J_{1cp} (kJ m^{-2})	4.56	4.42	4.68	4.29	4.23	4.53
D_{ca} (mm)	1.42	1.42	1.43	1.41	1.48	1.47
D_{cr} (mm)	1.22	1.39	1.41	1.35	1.29	1.32
With V-shaped side groove						
Thickness B (mm)	4	6	8	10	12.5	15
D_{cl} (mm)	1.51	1.44	1.53	1.50	1.51	1.51
J_{1cl} (kJ m^{-2})	6.60	6.02	6.38	6.31	6.18	6.34
D_{cp} (mm)	1.34	1.39	1.34	1.36	1.38	1.25
J_{1cp} (kJ m^{-2})	5.09	5.37	4.91	5.21	5.30	4.45
D_{ca} (mm)	1.36	1.40	1.39	1.43	1.38	1.31

[a] D_c: critical initial displacement; (l) from the plot of hysteresis energy *versus* displacement by using the linear propagation line; (p) from the plot of hysteresis energy *versus* displacement by using the power-law propagation line; (a) from the plot of the measured crack growth length *versus* displacement; (r) from the plot of hysteresis ratio *versus* displacement

energy and the corresponding J *versus* the crosshead displacement for PC/ABS samples with $B = 8$ mm. The critical initiation displacement D_{c1} is located at the intersection between the blunting line and the linear crack propagation line. (The validity crosshead displacement window is chosen according to the related crack growth length (Δa), ranging from 0.1 to 0.8 mm.) Alternatively, the critical displacement D_{cp} is located at the intersection between the blunting line and the second-order-power-law crack propagation line. In this case, the validity crosshead displacement window is chosen according to the corresponding crack growth length (Δa) and ranges from 0.1 to 1.20 mm. As soon as the critical displacement (D_{c1} or D_{cp}) is located, the corresponding J_{1c} value (J_{1cl} or J_{1cp}) is then determined from the J *versus* crosshead displacement curve. The values obtained for D_{cl}, D_{cp}, J_{1cl}, and J_{1cp} are summarized in *Table 4*. Since the measurement of crack growth length (Δa) is no longer necessary in this present method, the hysteresis energy method is relatively easier to carry out than the ASTM E813 methods. In a direct comparison of the results obtained from this hysteresis energy method with those from the ASTM E813-81 and E813-87 procedures, the J_{1c} values of the PC/ABS blend obtained from the hysteresis energy method are fairly close to those found from the E813-81 method (see *Table 2*), but are significantly lower (60–80%) than those from the E813-87 method (*Table 3*). The J_{1cp} values are closer to the J_{1c} values obtained from the E813-81 method than are the J_{1cl} values. The critical initiation displacement obtained at the interception between the blunting line and the second-order-power-law crack propagation line (D_{cp}) probably gives a more precise location of the true crack initiation than that obtained from the interception between the blunting line and the linear crack propagation line (D_{cl}), as described in our previous paper[44]. The main difference in these results is the number of valid data points used. *Figure 13* shows plots of J_{1cp} *versus* specimen thickness for PC/ABS specimens with and without the V-shaped side grooves. The specimens with side grooves have slightly higher J_{1cp} values than those without grooves. The critical J value determined by this unconventional hysteresis energy method has as its physical meaning the onset of crack extension, rather than that based on the theoretically predicted blunting line (as in ASTM E813-81) or that based on an arbitrarily chosen engineering definition (as in ASTM E813-87).

A typical plot of the crack growth length Δa *versus* crosshead displacement (D_{ca}) is shown in *Figure 14* for

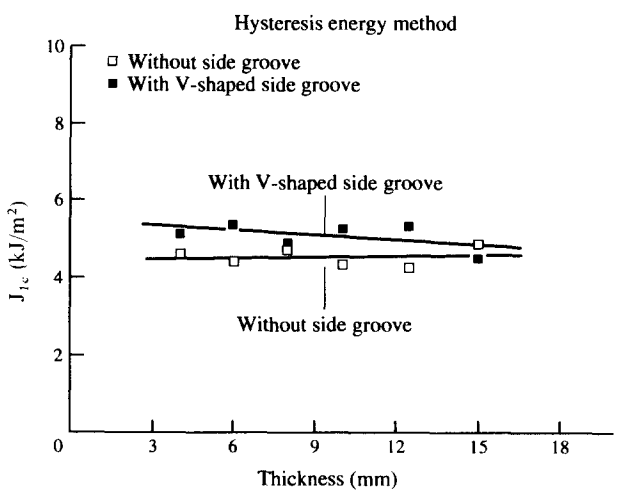

Figure 13 Plots of critical fracture toughness J_{1c} *versus* thickness obtained using the hysteresis energy method for PC/ABS samples with and without V-shaped side grooves

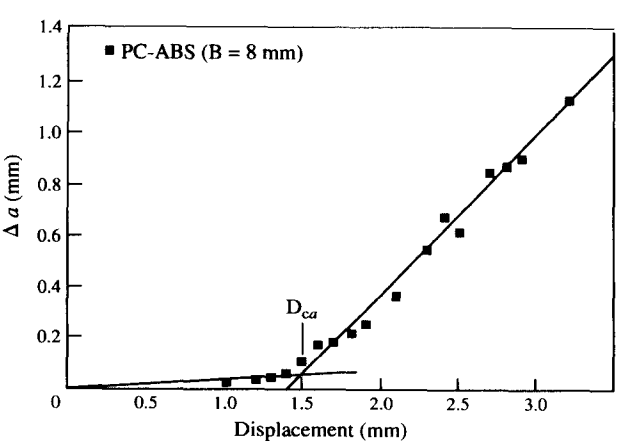

Figure 14 Plot of the true crack growth length (Δa) *versus* displacement for PC/ABS samples with $B = 8$ mm

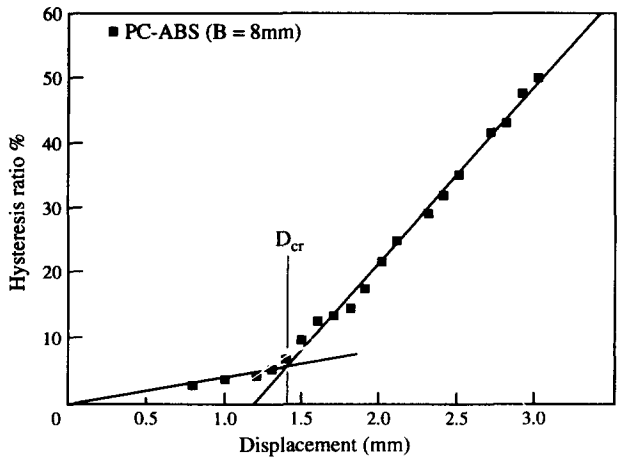

Figure 15 Plot of the hysteresis ratio *versus* displacement for PC/ABS samples with $B = 8$ mm

samples with $B = 8$ mm, in which the critical and true initiation displacement is now located at the intersection of the two naturally formed linear regression lines. *Figure 15* shows the plot of hysteresis ratio *versus* crosshead displacement using results obtained from the same set of samples ($B = 8$ mm). The critical displacement, D_{cr}, is again determined at the intersection from these two naturally formed linear regression lines. This D_{cr} value can also be considered as representing the true onset of critical initiation displacement. The D_{cr} values obtained for different thicknesses are summarized in *Table 4*. It is interesting to note that all of these critical displacement values, obtained from the three methods, i.e. the hysteresis energy, the hysteresis ratio, and the crack growth length *versus* displacement, are fairly close (*Table 4*), and are also independent of the specimen thickness. This indicates that the critical initiation displacement determined from the hysteresis methods (energy or ratio) does indeed represent the onset of crack extension.

The size criterion of specimens

ASTM E813 specifies that for a valid J_{1c} measurement the size criterion requirements of equation (10) must be met. The dJ/da values obtained according to the linear regression R-curves of ASTM E813-81 are summarized in *Table 5*. The tearing modulus (see equation (11)), T_m, is used to describe the stability of the crack growth. *Table 5* shows that the T_m values of both sample geometries are almost independent of the specimen thickness. In order for the J–Δa data to be regarded as an intrinsic property of the material, independent of specimen size, the criterion, ω (see equation (12)) > 10 must be met. In this paper, such a criterion is met for all samples in both specimen geometries (see *Table 5*). Other size criterion parameters (B, $(W-a)$, $W > 25$ (J_{1c}/σ_y)), according to the ASTM E813 methods for a valid J_{1c}, are all satisfied, as shown in *Table 5*. The size criteria for J testing allow for the use of significantly smaller specimen dimensions than those required for LEFM. *Table 5* summarizes various size criterion values for valid J_{1c} testing and all these criteria are essentially met in this study.

Further discussion

A sharply defined primary plastic zone, plus a secondary plastic zone ahead of the crack tip can be clearly observed in the optical photograph shown in *Figure 2a*. The sizes of both plastic zones increase with the increases in either crack growth length or crosshead deformation displacement. Lengths of both the primary plastic zone (r_{PPZ}) and the secondary plastic zone (r_{SPZ}) (as shown in *Figure 2c*) along the crack line were measured from an optical micrograph, and the results obtained are summarized in *Table 6*. *Figure 16* shows plots of the lengths of both primary and secondary plastic zones *versus* the crosshead displacement for PC/ABS samples with $B = 8$ mm. The dimensions of both plastic zones increase with an increase in the deformation displacement. The growth of the plastic zone increases with an increase in temperature under conditions of equal deformation displacement (data not shown) because of a lower yield stress at higher temperatures. It was postulated earlier that a LEFM parameter[45–47] could be used to characterize the fracture behaviour of toughened materials by assuming the crack initiation to be occurring shortly after the onset of non-linearity. The stress intensity

Table 5 The size criterion requirements for valid J_{1c} values for PC/ABS specimens with and without V-shaped side grooves

Without side groove						
Thickness B (mm)	4	6	8	10	12.5	15
dJ/da	14.5	12.6	16.6	16.7	17.7	16.2
$25(J_{1c}/\sigma_y)$	2.07	2.34	2.32	2.38	2.10	1.92
T_m[a]	14.2	12.3	16.2	16.3	17.3	15.8
ω parameter[b]	38.1	29.3	40.3	38.1	45.7	45.6
$\omega > 10$	Yes	Yes	Yes	Yes	Yes	Yes
Plane strain	Yes	Yes	Yes	Yes	Yes	Yes
With V-shaped side groove						
Thickness B (mm)	4	6	8	10	12.5	15
dJ/da	15.7	16.4	18.6	16.3	17.9	15.9
$25(J_{1c}/\sigma_y)$	3.56	2.94	2.31	2.48	1.97	1.87
T_m[a]	15.4	16.0	18.2	15.9	17.4	15.6
ω parameter[b]	23.9	30.9	43.6	35.6	49.1	46.2
$\omega > 10$	Yes	Yes	Yes	Yes	Yes	Yes
Plane strain	Yes	Yes	Yes	Yes	Yes	Yes

[a] $T_m = (E/\sigma_y^2)(dJ/da)$

[b] $\omega = [(W-a)/J_{1c}](dJ/da)$

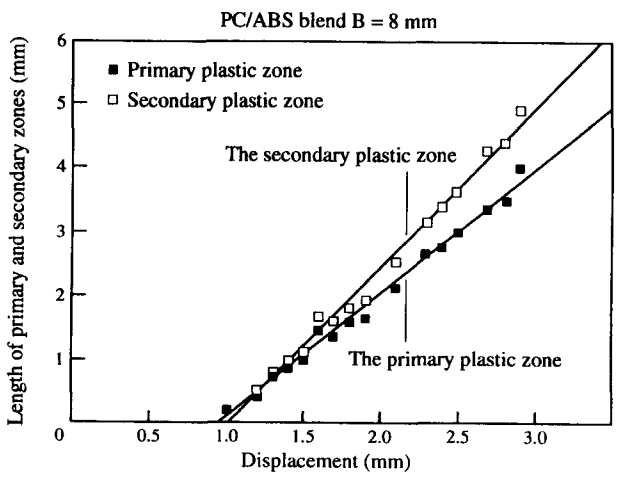

Figure 16 Plots of length of the primary plastic and secondary plastic zones *versus* displacement for PC/ABS samples with $B = 8$ mm

Table 6 Summary of the J data obtained for a typical PC/ABS blend with $B=8$ mm

D (mm)	r_{PPZ}[a] (mm)	r_{SPZ}[b] (mm)	K value[c] (MPa m^{-1})			J[d] (kJ m^{-2})		
			$m=1$	$m=\sqrt{3}$	$m=3$	$m=1$	$m=\sqrt{3}$	$m=3$
1.0	0.164	0.19	0.94	1.62	2.82	0.37	1.12	3.37
1.2	0.402	0.45	1.47	2.54	4.41	0.92	2.75	8.26
1.3	0.772	0.76	2.03	3.53	6.11	1.76	5.29	15.87
1.4	0.859	0.96	2.15	3.72	6.45	1.96	5.88	17.66
1.5	0.994	1.05	2.31	4.00	6.94	2.27	6.81	20.43
1.6	1.451	1.62	2.79	4.83	8.38	3.31	9.93	29.81
1.7	1.342	1.56	2.68	4.65	8.05	3.06	9.18	27.55
1.8	1.575	1.76	2.90	5.03	8.72	3.58	10.76	32.28
1.9	1.622	1.88	2.95	5.11	8.86	3.70	11.10	33.31
2.1	2.089	2.46	3.35	5.81	10.06	4.77	14.32	42.97
2.3	2.600	3.15	3.74	6.48	11.22	5.94	17.82	53.46
2.4	2.726	3.37	3.82	6.62	11.48	6.21	18.64	55.92
2.5	2.985	3.60	4.00	6.93	12.02	6.80	20.42	61.27
2.7	3.364	4.21	4.25	7.36	12.76	7.67	23.02	69.08
2.8	3.477	4.34	4.32	7.48	12.96	7.92	23.78	71.34
2.9	3.940	4.85	4.60	7.97	13.81	9.00	27.00	81.01
3.0	3.852	4.99	4.55	7.88	13.65	8.79	26.38	79.16

[a] r_{PPZ} = length of the primary plastic zone
[b] r_{SPZ} = length of the secondary plastic zone
[c] $K=(r_p/0.393)^{1/2}m\sigma_y$
[d] $J=K^2(1-\nu^2)/E$

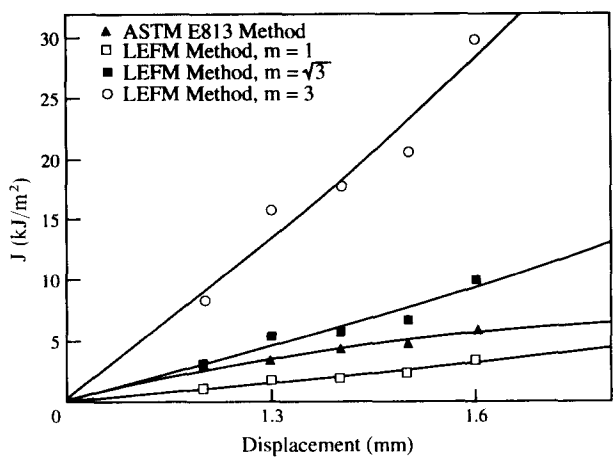

Figure 17 Plots of J *versus* displacement for PC/ABS samples using the ASTM E813 method and the LEFM method with various constraint factors (see text for details)

factor, K, is calculated by using the following equation:

$$K = Y\sigma_y a^{1/2} \tag{20}$$

where Y is a geometrical factor, and $a=a_0+\Delta a$. The Dugdale model predicts the length of the plastic zone, r_p (ahead of the crack tip) as follows:

$$r_p = 0.393\left(\frac{K}{m\sigma_y}\right)^2 \tag{21}$$

where m is the plastic constraint factor. In this paper, the K values are calculated from equation (21) by using the length of the observed primary plastic zone. Three constraint factors, $m=1$, $3^{1/2}$, or 3 are chosen to calculate the K values, and these are summarized in *Table 6*. Under LEFM conditions, the K value can be converted into the J (J_c) value by using the following equation:

$$J(J_c) = K^2(1-\nu^2)/E \tag{22}$$

Three sets of the calculated J (J_c) values obtained from the corresponding K values (based on $m=1$, $3^{1/2}$, and 3) are also listed in *Table 6*. *Figure 17* shows plots of J *versus* the crosshead displacement using results obtained from the ASTM E813-81 method and this LEFM approach with various constraint factors, using data points taken up to crack initiation to ensure LEFM conditions. The crack tip constraint factor, m, obtained from the J–D curve based on the ASTM E813 method, is determined to be approximately equal to $2^{1/2}$.

CONCLUSIONS

From the optical photographs of the deformed specimens, two plastic zones can be identified, i.e. the interior one is the primary plastic zone while the outer one is the secondary plastic zone. The sizes of both plastic zones (r_{PPZ} and r_{SPZ}) increase with an increase in the deformation displacement and the temperature of testing. The critical fracture toughness (J_{1c}) values obtained from the hysteresis energy method are comparable to those obtained from the E813-81 method but are about 60–90% lower than those obtained from the E813-87 method. The critical J values (from the ungrooved specimens) obtained from the ASTM E813-81, E813-87, and hysteresis energy methods are nearly independent of the sample thickness. However, the critical J values for specimens with V-shaped side grooves are higher than those without the grooves for thinner specimens, but the difference decreases with an increase in the specimen thickness. The critical displacements obtained from these three methods,

i.e. the hysteresis energy, hysteresis ratio, and the crack growth length *versus* displacement, are fairly close in value and are independent of sample thickness. This result indicates that the critical initiation displacement determined from the hysteresis methods (energy or ratio) does indeed represent the onset of crack extension. The crack tip constraint factor of $m=2^{1/2}$ for an ungrooved PC/ABS blend specimen with $B=8$ mm was obtained by using the Dugdale model and measured sizes of the primary plastic zones.

ACKNOWLEDGEMENTS

The authors are grateful to the National Science Council of the Republic of China for financial support of this work.

REFERENCES

1 ASTM Standard E399-78 in 'Annual Book of ASTM Standards', part 10, ASTM, Philadelphia, PA, 1978, p. 540
2 Rice, J. R. *J. Appl. Mech.* 1968, **35**, 379
3 Begley, J. A. and Landes, J. D. ASTM STP 514, 1972, 1
4 Landes, J. D. and Begley, J. A. ASTM STP 560, 1974, 170
5 Chan, M. K. V. and Williams, J. G. *Int. J. Fract.* 1983, **19**, 145
6 Chan, M. K. V. and Williams, J. G. *Polym. Eng. Sci.* 1981, **21**, 1019
7 Hashemi, S. and Williams, J. G. *Polymer* 1986, **27**, 384
8 Huang, D. D. and Williams, J. G. *J. Mater. Sci.* 1987, **22**, 2503
9 So, P. K. and Broutman, L. J. *Polym. Eng. Sci.* 1986, **26**, 1173
10 Moskala, E. J. and Tant, M. R. *Polym. Mater. Sci. Eng.* 1990, **63**, 63
11 Rimnac, C. M., Wright, T. M. and Klein, R. W. *Polym. Eng. Sci.* 1988, **28**, 1586
12 Narisawa, I. *Polym. Eng. Sci.* 1987, **27**, 41
13 Parker, D. S., Sue, H. J., Huang, J. and Yee, A. F. *Polymer* 1990, **31**, 2267
14 Haddaoui, N., Chudnovsky, A. and Moet, A. *Polymer* 1986, **27**, 1337
15 Tung, I. C. *Polym. Bull.* 1991, **25**, 253
16 Narisawa, I. and Takemori, M. T. *Polym. Eng. Sci.* 1989, **29**, 671
17 Huang, D. D. and Williams, J. G. *Polym. Eng. Sci.* 1990, **30**, 1341
18 Huang, D. D. *Polym. Mater. Sci. Eng.* 1990, **63**, 578
19 Rice, J. R., Paris, P. C. and Merkle, J. G. ASTM STP 536, 1973, 231
20 Westerlind, B. S., Carlsson, L. A. and Andersson, Y. M. *J. Mater. Sci.* 1991, **26**, 2630
21 Afluri, S. N., Ankagami, M. and Chen, W. H. ASTM STP 631, 1977, 42
22 Shin, C. G., Germann, M. D. and Kumar, V. *J. Press. Vessel Piping* 1981, **9**, 159
23 ASTM Standard E813-81 in 'Annual Book of ASTM Standards', part 10, ASTM, Philadelphia, PA, 1981, p. 810
24 ASTM Standard E813-87 in 'Annual Book of ASTM Standards', part 10, ASTM, Philadelphia, PA, 1987, p. 968
25 Seidler, S. and Grellmann, W. *J. Mater. Sci.* 1993, **28**, 4078
26 Mai, Y. W. and Cotterell, B. *J. Mater. Sci.* 1980, **15**, 2296
27 Mai, Y. W. and Cotterell, B. *Eng. Fract. Mech.* 1985, **21**, 123
28 Wu, J., Mai, Y. W. and Cotterell, B. *J. Mater. Sci.* 1993, **28**, 3373
29 Zhou, Z., Landes, J. D. and Huang, D. D. *Polym. Eng. Sci.* 1994, **34**, 128
30 Chung, W. N. and Williams, J. G. ASTM STP 1114, 1991, 320
31 Lee, C. B. and Chang, F.-C. *Polym. Eng. Sci.* 1992, **32**, 792
32 Lee, C. B., Lu, M.-L. and Chang, F.-C. *Polym. Mater. Sci. Eng.* 1992, **64**, 510
33 Lee, C. B., Lu, M.-L. and Chang, F.-C. *J. Appl. Polym. Sci.* 1993, **47**, 1867
34 Lee, C. B., Lu, M.-L. and Chang, F.-C. *J. Chin. Inst. Chem. Eng.* 1992, **23**, 305
35 Lu, M.-L., Lee, C. B. and Chang, F.-C. *Polym. Eng. Sci.* in press
36 Sumpter, J. D. and Turner, C. E. *Int. J. Fract.* 1973, **9**, 320
37 Paris, P. C., Tada, H., Zahoor, A. and Ernst, H. ASTM STP 668, 1979, 5
38 Andrews, E. H. *J. Mater. Sci.* 1974, **9**, 887
39 Andrews, E. H. and Fukahori, Y. *J. Mater. Sci.* 1977, **12**, 1307
40 Chang, F.-C. and Hsu, H. C. *J. Appl. Polym. Sci.* 1991, **43**, 1025
41 Chang, F.-C. and Yang, M. Y. *Polym. Eng. Sci.* 1990, **30**, 543
42 Chang, F.-C. and Hsu, H, C. *J. Appl. Polym. Sci.* 1993, **47**, 2195
43 Chang, F.-C. and Hsu, H.C. *J. Appl. Polym. Sci.* 1994, **52**, 1891
44 Lu, M.-L., Lee, C. B. and Chang, F.-C. *J. Mater. Sci.* in press
45 Williams, J. G. 'Fracture Mechanics of Polymers', Ellis Horwood, Chichester, 1987
46 Strebel, J. J. and Moet, A. *J. Mater. Sci.* 1992, **27**, 2981
47 Moskala, E. J. *J. Mater. Sci.* 1992, **27**, 4883